

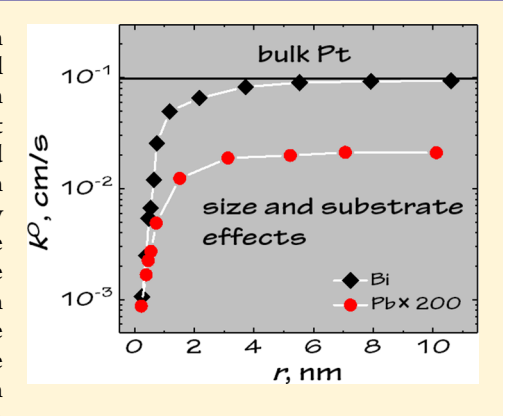
# Probing Size and Substrate Effects on the Hydrogen Evolution Reaction by Single Isolated Pt Atoms, Atomic Clusters, and **Nanoparticles**

Min Zhou, Shujuan Bao, and Allen J. Bard\*

Center for Electrochemistry, Department of Chemistry, The University of Texas at Austin, Austin, Texas 78712, United States

Supporting Information

ABSTRACT: We report the catalytic activity of a single, isolated Pt deposit on Bi and Pb supports to probe the size and substrate effects on the electrochemical hydrogen evolution reaction (HER). Deposits were made electrolytically by an atom-by-atom method in a controlled plating; we prepared an individual Pt deposit on Bi and Pb ultramicroelectrodes (UMEs) such as a single isolated atom, clusters containing one to five Pt atoms, and nanoparticles to about 10 nm radius. A steady-state voltammogram on the single Pt deposits is observed by electrocatalytic amplification of the HER, with a negligible contribution by the HER at the substrate UME. A single Pt atom can act as an electrode for the HER, showing a diffusion-limiting current plateau in the voltammogram that can be used to estimate the radius of a single deposit. We simulated the voltammograms of the individual deposits, assuming the Volmer step of the HER is appropriate for a Pt cluster deposit, to obtain kinetic parameters for each deposit. The HER kinetics increases as the particle radius increases from ~0.2 to



~4 nm for Bi and Pb substrates and then reaches a limiting plateau. The limiting kinetics on the Bi substrate approaches that of bulk Pt while that on the Pb substrate is much smaller.

#### INTRODUCTION

We recently reported an atom-by-atom basis method to plate isolated Pt atoms and clusters on the Bi ultramicroelectrode (UME) from femtomolar H<sub>2</sub>PtCl<sub>6</sub> solution and compared their electrocatalytic activity toward the hydrogen evolution reaction (HER) in a semiquantitative way. This demonstrated that electrochemistry is a powerful tool to prepare and characterize single isolated catalytic atoms and clusters.2 There are few studies of isolated, single atoms but many studies of the catalytic properties of ensembles of single atoms or clusters.<sup>3-6</sup> Generally, the evidence that these atoms exist on a surface as dispersed atoms is through high-resolution scanning transmission electron microscopy (STEM).<sup>3</sup> Anderson and coworkers size-selectively sputtered Pt clusters on a carbon surface and measured the effect of cluster size on the oxygen reduction reaction (ORR) kinetics. Sun and co-workers used atomic layer deposition (ALD) to prepare ensembles of single Pt atoms and studied the effect of size on the HER.<sup>5</sup> Other groups have looked at the catalysis of single Pt atom ensembles under different circumstances, such as CO oxidation on FeO<sub>x</sub> substrates<sup>3</sup> and the HER on Pt-doped MoS<sub>2</sub> substrates.<sup>4</sup> These measurements are made with bulk quantities of atoms or clusters and not on single isolated ones. In many cases, the authors did not account for possible Ostwald ripening of the atoms into clusters on the substrate surfaces with time, especially when catalytic reactions were being driven.8 In addition, they did not consider individual catalyst proximity in an ensemble when evaluating the effects of size and support on the electrocatalytic activity.

Here, we report an approach to characterizing a single isolated catalyst deposit that is free of the above shortcomings. We also provide a better measure of electrochemical kinetics than in the previous work. We adopt an atom-by-atom methodology to electrodeposit an isolated single Pt atom, atomic cluster, or nanoparticle (NP) on Bi and Pb UMEs, and characterize their electrocatalysis by steady-state voltammetry, i.e., size and substrate effects. The first study describes the methodology in detail.1 Briefly:

- 1. Single Pt atoms are deposited from solutions of very small (fM) concentrations of H<sub>2</sub>PtCl<sub>6</sub>, slowing the deposition rate to about one Pt atom every 10 s. As described below, the number of active sites on the UME are so small that deposition and growth at more than one site is very improbable.
- 2. The deposit is characterized by voltammetry, which yields a diffusion limiting current that is proportional to the deposit size and potential that is determined by heterogeneous electron transfer (ET) kinetics of the HER.

## RESULTS AND DISCUSSION

Bi and Pb UMEs. The nanometer size Bi and Pb UMEs were fabricated by the technique described previously (see the

Received: December 14, 2018 Published: April 24, 2019



Supporting Information). The smaller size of the UMEs is more favorable since they can give smaller voltammetric backgrounds. Parts a and B of Figure 1 show CVs of Bi and Pb UMEs in 40 mM

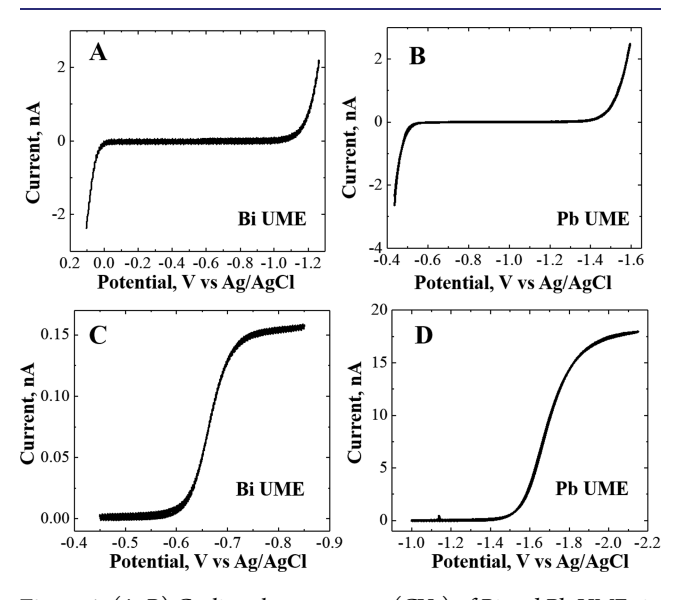


Figure 1. (A, B) Cyclic voltammograms (CVs) of Bi and Pb UMEs in 40 mM HClO<sub>4</sub> and 0.2 M NaClO<sub>4</sub> solution. (C, D) CVs of Bi and Pb UMEs in 5 mM MVCl<sub>2</sub>, 0.2 M KCl, and 40 mM HClO<sub>4</sub>, 0.2 M NaClO<sub>4</sub> solutions, respectively. The voltammograms of forward and backward scan were retraceable for A-D. The solutions were deaerate, and the scan rates were 50 mV/s.

HClO<sub>4</sub> and 0.2 M NaClO<sub>4</sub> solution in which the positive and negative limits were respectively controlled by the metal oxidation and HER. Note that Pb is oxidized more easily and has a significantly higher HER overpotential than Bi. 12 As such, both metals can be used as the catalytically inactive supports to detect HER on the catalytically active Pt deposits. As demonstrated previously, the Bi UME can be characterized by use of methyl vilogen (MV<sup>2+</sup>) reduction voltammetry (Figure

However, this redox probe was not applicable to the voltammetric measurement of Pb UME because it chemically oxidizes the Pb metal. Alternatively, proton reduction voltammetry was used to calibrate the Pb UME in 40 mM HClO<sub>4</sub> and 0.2 M NaClO<sub>4</sub> solution (Figure 1D). To estimate the size of both UMEs, the steady-state voltammetry on a standard Pt UME (5  $\mu$ m radius) were obtained accordingly in the MV<sup>2+</sup> and H<sup>+</sup> solutions, showing the diffusion-limiting currents of 5.95 and 718 nA. Knowing the ratio between the corresponding diffusion limiting currents, we determine the radii of Bi and Pb UMEs as 126 and 123 nm, respectively.

Single Pt Atoms. Previously, we demonstrated the nucleation of a single Pt atom on a UME by electrodeposition. At a potential where the deposition is diffusion controlled and assuming a strong interaction between the deposited Pt atoms and the substrate, the deposition frequency is the same as the diffusion-controlled frequency of the PtCl<sub>6</sub><sup>2-</sup> arrival at the electrode surface as described by<sup>13</sup>

$$f = 4DcaN_{A} \tag{1}$$

where D and c are the diffusion coefficient  $(1.2 \times 10^{-5} \text{ cm}^2/\text{s}^{14})$ and the concentration of PtCl<sub>6</sub><sup>2-</sup>, N<sub>A</sub> is Avogadro's number  $(6.02E23 \text{ mol}^{-1})$ , and a is the radius (ca. 120 nm) of the prepared Bi and Pb UMEs. Under a loading frequency of 0.1 Hz

(or an average of 1 atom every 10 s), the plating solution should contain ca. 300 fM H<sub>2</sub>PtCl<sub>6</sub> in water for a 120 nm radius UME. In fact, the plating events of Pt<sub>n</sub> ( $n \ge 0$ ) occur randomly within a specified time, which can be described by Poisson statistics

$$P(k,\lambda) = \frac{\lambda^k e^{-\lambda}}{k!} \tag{2}$$

where  $\lambda$  is the expected or most probable value (e.g., for a 10 s plating,  $\lambda = 1$ ; for 20 s,  $\lambda = 2$ ...) and  $P(k, \lambda)$  is the probability of kwhere  $\lambda$  is the expected value. Here, during a 10 s plating, the probability of preparation of a single Pt atom can be P(1, 1) =36%. While the current or charge of the electrodeposition of a single atom is too small to measure, by using the HER inertness of Bi and Pb UMEs, a single Pt atom can be detected in voltammetry via electrocatalytic amplification by the HER at a suitable proton concentration. The solution used was 40 mM HClO<sub>4</sub> and 0.2 M NaClO<sub>4</sub> with oxygen removed. If we consider a diffusion exclusion zone around an atom, we can assume a hemispherical shape to estimate the radius<sup>13</sup>

$$r = i_{\rm l}/2\pi n F D_{\rm H}^{+} c_{\rm H}^{+} \tag{3}$$

where  $i_1$  is the diffusion-limiting current obtained of the steadystate voltammogram, r is the equivalent radius of the deposit, n = 11 is the electron number, F = 96485 C/mol is the Faraday constant, and  $D_{\rm H}^{+} = 9.3 \times 10^{-5} \, {\rm cm}^{2}/{\rm s}^{16}$  and  $c_{\rm H}^{+} = 40 \, {\rm mM}$  are, respectively, the diffusion coefficient and concentration of proton.

The assumption that all deposits can be treated as hemispherical shapes is based on the empirical correlation between the limiting current and the assumed size of the cluster, Pt<sub>n</sub>, with n = 1 for the smallest, n = 2 for the next, etc., providing the best linear behavior. Note also that deposits like atoms or clusters show significant quantum effects and strong interactions with the support, 5,11 so that they cannot be treated like the classical nanoelectrodes. As such, it is impossible to establish the electrified interface at such small atoms or clusters and no conventional diffuse layer effect 18 could be expected

For the Bi substrate, for 16 trials of 10 s deposition, 5 times showed the smallest diffusion-limiting current at  $55 \pm 9$  pA in the steady-state voltammograms, corresponding to a size of 0.25  $\pm$  0.04 nm. This value is similar to the accepted platinum lattice radius. Similarly, for the Pb substrate, 4 times in 14 trials showed the smallest diffusion-limiting current at 53  $\pm$  8 pA, corresponding to a size of  $0.24 \pm 0.03$  nm. The observed probabilities of the above events were 31% and 28%, which are close to the theoretical prediction, P(1,1) = 36%. Moreover, no voltammogram with a limiting current within the standard deviation was ever seen between these smallest values and background. Such voltammograms were also never seen on Bi or Pb without a Pt electrodeposition step. Thus, from the estimated radius and the statistical prediction, we propose that this minimum deposit is an isolated single Pt atom.

Typical HER voltammograms of a single isolated Pt atom on Bi and Pb UMEs along with the substrate background are shown in Figure 2. A diffusion-limited voltammetric plateau on one Pt atom occurs before the HER begins on the substrate. A single Pt atom deposited on Bi and Pb is not stable. After a single scan through the plateau region, even without a reverse scan, no HER voltammogram was seen in a new scan in about 70% of the trials. The stability depends on the bonding between the atom and the substrate and perhaps the adsorption of blocking impurities

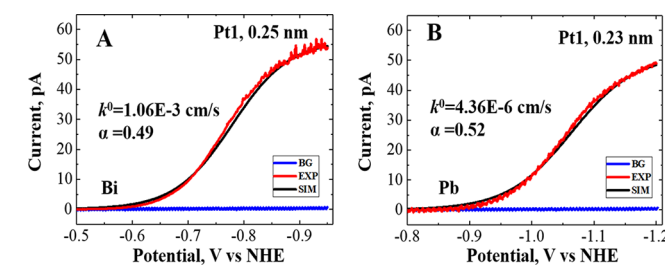


Figure 2. (A, B) Forward scan voltammograms of HER on a single Pt atom deposited on Bi and Pb UMEs. The detection solution contained 40 mM HClO<sub>4</sub> and 0.2 M NaClO<sub>4</sub>. The scan rates were 50 mV/s. The fitting standard deviations show 1.2% and 1.5% for panels A and B, respectively. The labels of BG, EXP, and SIM refer to the background, experiment, and simulation discussed below.

from the solution. This was found with continuous voltammetric and intermittent single-segment scanning (30 s interval between trials). For both Bi and Pb, we observed that the single atom voltammogram decays to background 70% of the time after a single sweep or gets missing mostly when the deposit was kept in the detection solution at open circuit potential.

We also want to compare the heterogeneous ET kinetics at a single atom (and small clusters) to that of bulk Pt. In our previous paper, this was shown in a semiquantitative way by reporting the overpotential at a given current density. Here, we attempt a treatment that is more quantitative by fitting the experimental results to the Butler-Volmer equation. For simplicity, we assume that the HER at atoms, clusters, and NPs follows the same general mechanism as the HER on bulk Pt, i.e., the 1e Volmer step to form a H atom adsorbed on Pt 19

$$H^+ + e^- \to H^{\bullet}_{ads} \tag{4}$$

followed by the Tafel  $(2 H_{ads}^{\bullet} \rightarrow H_2)$  or Heyrovsky  $(H_{ads}^{\bullet} + H_2)$  $\rightarrow$  H<sub>2</sub>) step. These latter steps are usually taken as very rapid, so that the Volmer step is rate-determining, leading to a 1e equation. These steps may be slower at atoms and small clusters, but the experiment suggests that they are sufficiently rapid to show electrocatalytic amplification by H2 evolution. We thus hypothesize for all cases an  $E_{H/H}^{0}$  and  $E_{ads}^{0} = 0$  V vs NHE and calculate two parameters ( $k^0$  and  $\alpha$ ) to represent the kinetics. Note that application of the Butler-Volmer equation to a single atom or cluster has yet to be demonstrated, and a more rigorous analysis may be possible. 14,18 However, the experimental data when fit to the Butler-Volmer equation with two adjustable parameters is quite good. Assuming a hemispherical geometry, we can simulate the steady-state voltammogram with Digielch software and compare these to the experimental data. The results show, for a single Pt atom,  $k^0 = 1.06 \times 10^{-3}$  cm/s and  $\alpha =$ 0.49 for the Bi substrate and  $k^0 = 4.36 \times 10^{-6}$  cm/s and  $\alpha = 0.52$ for the Pb substrate with a fitting standard deviation (SD) of 1.2% and 1.5%. The largely different HER kinetics on a single Pt atom supported on different substrates will be considered below.

**Single Pt Atomic Clusters.** In this paper, we define clusters as deposits with radii less than  $\sim 1$  nm. For electrodeposition, the active nucleation site density on metal substrate surfaces  $(N_0)$ are in the range  $10^4 < N_0 < 10^{10}$  cm<sup>-2</sup>, and thus, typically  $N_0$  does not exceed  $\sim 10^8$  cm<sup>-2</sup>. The expected number of active sites on the surface of a  $\sim 120$  nm-radius electrode is  $\ll 1.^{23}$  As demonstrated previously,  $^{1,16,24}$  metal electrodeposition on a small UME showed a nucleation and growth of a single Pt deposit, rather than multiple deposits. Such results suggest that the deposited atoms are concentrated at the lowest stabilized

energy of a site by thermodynamic and potential induced surface motion.<sup>25,26</sup>

According to the Poisson prediction, the distribution of cluster sizes and probabilities of a 10 s plating trial are  $Pt_0$  (36%), Pt<sub>1</sub> (36%), Pt<sub>2</sub> (18%), and Pt<sub>3</sub> (6%) and for 20 s Pt<sub>0</sub> (14%), Pt<sub>1</sub> (27%), Pt<sub>2</sub> (27%), Pt<sub>3</sub> (18%), Pt<sub>4</sub> (9%), and Pt<sub>5</sub> (4%). To prepare a single  $Pt_n$  ( $n \le 5$ ) cluster on the Bi and Pb substrates, we carried out multiple trials of 20 s plating. For the Bi substrate, in 23 trials of plating, 5 times of voltammetric detections gave the smallest diffusion-limiting current of  $57 \pm 8 \text{ pA}$ ; 7 times gave that of 93  $\pm$  8 pA; 3 times gave that of 112  $\pm$  9 pA; 2 time gave that of  $122 \pm 11$  pA; 1 time gave that of 147 pA; 5 times gave the background without deposit. These trials of voltammograms are all listed in Figure S1.

From eq 3, the equivalent radius of a single cluster can be estimated from the obtained diffusion-limiting current. The estimated radius and frequency of single clusters formed by the 20 s plating are  $0.25 \pm 0.04$  nm (22%),  $0.40 \pm 0.03$  nm (30%),  $0.48 \pm 0.04$  nm (13%),  $0.54 \pm 0.05$  nm (9%), and 0.65 nm (4%). When n is small in a single  $Pt_n$  cluster, assuming that the deposit has a 2D structure and the equivalent area approximation is applicable, the number of atoms can be estimated as

$$n = \left(r_n/r_1\right)^2 \tag{5}$$

where  $r_1$  is the effective radius of a single Pt atom. Figure 3A shows a reasonable agreement between the Poisson distribution

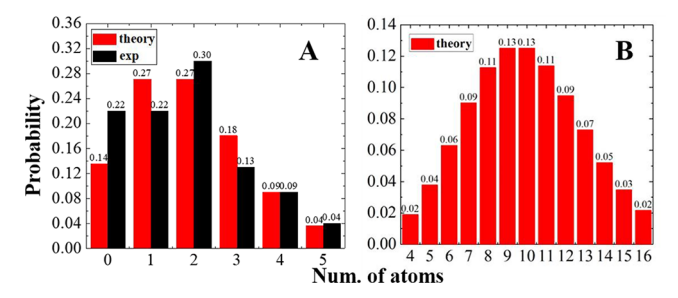


Figure 3. (A) Histogram of the calculated number of atoms overlaid with a Poisson distribution when the deposition time was 20 s for the Bi substrate. The data includes 23 total trials of plating. (B) Predicted Poisson distribution for a 100 s plating. Experimental conditions are the same as in Figures 1 and 2

and the experiments (23 trials) for the 20 s plating on Bi. Figure 3B depicts that the predicted Poisson distribution for a 100 s plating greatly broadens compared to that for the 20 s plating, which makes it difficult to judge and recognize the identification of trials. As shown in Figure 4A,B, the 0.75 and 0.73 nm radius of clusters deposited on Bi and Pb from the 100 s plating cannot give the estimated number of atoms.

Typical HER voltammograms of single Pt<sub>n</sub> clusters on Bi and Pb UMEs are illustrated in Figure 4A,B, where the determined size and number of atoms are labeled. As the size of a single cluster  $(r_{NP})$  becomes large, the corresponding half-wave potential  $(E_{1/2})$  shifts positively. This is attributed to both increases in the deposit size (mass-transfer effect) and the kinetics (electrocatalytic activity) as shown in the following equation:

$$E_{1/2} = E^{0}_{H^{+}/H^{\bullet}ads} + RT/\alpha F \ln(r_{NP}k^{0}/D_{H^{+}})$$
 (6)

Apparently, the position of the half-wave potential can be regarded as the first criterion to discriminate voltammograms of atoms and clusters in the plating trials as shown in Figure 4A,B.

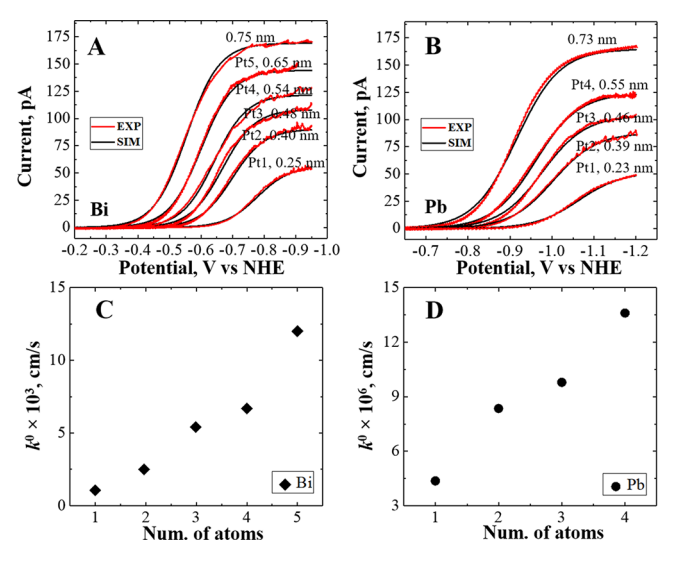


**Figure 4.** (A, B) Forward scan voltammograms of HER on a single Pt atom and a single cluster deposited on Bi and Pb UMEs. The detection solution contained 40 mM  $\rm HClO_4$  and 0.2 M  $\rm NaClO_4$ . The scan rates were 50 mV/s. (C, D) The extracted  $k^0$  as a function of the number of atoms in a single Pt, cluster on Bi and Pb substrates. The 0.75 and 0.73 nm radius of clusters deposited on Bi and Pb are from the 100 s plating and others are from the 10 s plating.

With Bi and Pb UMEs, an entire voltammetric curve can be obtained for the HER on a single cluster with no interference by the substrate material. As proposed for single atoms using the Volmer mechanism for a HER and the Bulter-Volmer equation for an ET kinetics, we calculated a steady-state voltammogram and compared it to the corresponding experimental steady-state voltammogram (Figure 4A,B). The  $k^0$  and  $\alpha$  determined are listed in Tables 1 and 2 for Bi and Pb substrates, respectively. For

Table 1. Parameters Determined from HER Voltammograms of Single Pt Deposits on Bi

|       |        |                     | $k^0$ and $lpha$ fitting |                       |      |                    |  |
|-------|--------|---------------------|--------------------------|-----------------------|------|--------------------|--|
| r, nm | $Pt_n$ | i <sub>l</sub> , pA | $E^0$ , V                | k <sup>0</sup> , cm/s | α    | SD, <sup>b</sup> % |  |
| 0.25  | $Pt_1$ | 56                  | 0                        | $1.06 \times 10^{-3}$ | 0.49 | 1.2                |  |
| 0.40  | $Pt_2$ | 90                  | 0                        | $2.50 \times 10^{-3}$ | 0.48 | 1.4                |  |
| 0.48  | $Pt_3$ | 108                 | 0                        | $5.41 \times 10^{-3}$ | 0.52 | 1.6                |  |
| 0.54  | $Pt_4$ | 121                 | 0                        | $6.70 \times 10^{-3}$ | 0.53 | 1.8                |  |
| 0.65  | $Pt_5$ | 146                 | 0                        | $1.20 \times 10^{-2}$ | 0.48 | 1.1                |  |
| 0.75  |        | 168                 | 0                        | $2.55 \times 10^{-2}$ | 0.47 | 1.2                |  |
| 1.18  |        | 264                 | 0                        | $4.97 \times 10^{-2}$ | 0.56 | 1.4                |  |
| 2.17  |        | 486                 | 0                        | $6.53 \times 10^{-2}$ | 0.61 | 1.2                |  |
| 3.72  |        | 833                 | 0                        | $8.23 \times 10^{-2}$ | 0.53 | 2.1                |  |
| 5.53  |        | 1238                | 0                        | $9.03 \times 10^{-2}$ | 0.52 | 1.4                |  |
| 7.92  |        | 1774                | 0                        | $9.24 \times 10^{-2}$ | 0.48 | 1.4                |  |
| 10.61 |        | 2376                | 0                        | $9.37 \times 10^{-2}$ | 0.46 | 1.5                |  |

<sup>a</sup>Assuming  $E^0 = 0$  V vs NHE. <sup>b</sup>The standard deviation of the curve fitting.

Bi and Pb substrates, as the number of atoms in a single cluster increases, the corresponding  $k^0$  increases concomitantly (Figure 4C,D). However, the  $k^0$  of similar size clusters on Bi is  $\sim 10^3$  times higher than that on Pb.

**Single Pt NPs.** Slightly different from the single cluster preparation, we used a relatively high concentration of  $H_2PtCl_6$  solution or a comparably long time to deposit a large Pt NP. The corresponding  $H_2PtCl_6$  concentration and plating time are

Table 2. Parameters Determined from HER Voltammograms of Single Pt Deposits on Pb

|       |        |                | $k^0$ and $lpha$ fitting |                       |      |                    |  |
|-------|--------|----------------|--------------------------|-----------------------|------|--------------------|--|
| r, nm | $Pt_n$ | $i_{\rm b}$ pA | $E^0$ , V                | k <sup>0</sup> , cm/s | α    | SD, <sup>b</sup> % |  |
| 0.23  | $Pt_1$ | 52             | 0                        | $4.36 \times 10^{-6}$ | 0.52 | 1.5                |  |
| 0.39  | $Pt_2$ | 88             | 0                        | $8.35 \times 10^{-6}$ | 0.61 | 1.2                |  |
| 0.46  | $Pt_3$ | 104            | 0                        | $9.79 \times 10^{-6}$ | 0.48 | 1.9                |  |
| 0.55  | $Pt_4$ | 124            | 0                        | $1.36 \times 10^{-5}$ | 0.45 | 1.1                |  |
| 0.73  |        | 165            | 0                        | $2.44 \times 10^{-5}$ | 0.52 | 1.6                |  |
| 1.52  |        | 344            | 0                        | $6.18 \times 10^{-5}$ | 0.50 | 1.0                |  |
| 3.13  |        | 708            | 0                        | $8.95 \times 10^{-5}$ | 0.57 | 1.0                |  |
| 5.22  |        | 1180           | 0                        | $1.03 \times 10^{-4}$ | 0.49 | 0.9                |  |
| 7.07  |        | 1598           | 0                        | $1.06 \times 10^{-4}$ | 0.53 | 1.1                |  |
| 10.12 |        | 2288           | 0                        | $1.08 \times 10^{-4}$ | 0.47 | 1.2                |  |
|       |        |                |                          |                       |      |                    |  |

<sup>a</sup>Assuming  $E^0 = 0$  V vs NHE. <sup>b</sup>The standard deviation of the curve fitting.

detailed in the SI. Even for the largest Pt NP ( $\sim$ 10 nm radius), the integrated charge produced is still too small to measure. <sup>16,24</sup> To identify the deposit size, we follow the strategy of electrocatalytic amplification by the HER. To avoid interference of  $\rm H_2$  bubble formation, a suitably low concentration of acid (40 mM HClO<sub>4</sub>) was chosen. To suppress bulk migration and diffuse-layer effects on the particle electrode, a sufficient amount of electrolyte (200 mM NaClO<sub>4</sub>) was used. Although the diffusion exclusion zone of proton is insignificant for a large particle, a hemispherical geometry is still adopted owing to its real structure from the electrodeposition.

Parts A and B of Figure 5 show the HER voltammograms of single Pt NPs on Bi and Pb substrates, where the corresponding

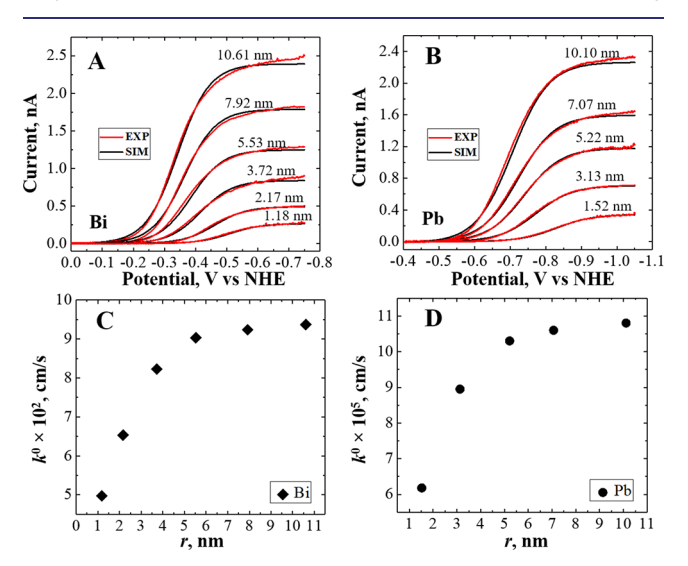


**Figure 5.** (A, B) Forward scan voltammograms of HER on a single Pt NP deposited on Bi and Pb UMEs. The solution contained 40 mM  $HClO_4$  and 0.2 M  $NaClO_4$ . The scan rates were 50 mV/s. (C, D) Extracted  $k^0$  as a function of the radius of a single Pt NP on Bi and Pb substrates.

radius are labeled inset. The size of Pt deposit ranges from ca. 1 to 10 nm. The half-wave potential shifts positively along with the size increases; when the particle size is comparable, the HER voltammogram on Bi is significantly more positive than that on Pb. Following the former HER model, we perform the curve fitting analysis on the obtained voltammograms. The extracted parameters such as  $k^0$  and  $\alpha$  are collected in Tables 1 and 2 for Bi

and Pb substrates, respectively. Here we have to judge the fitting accuracy for the  $k^0$ . For a 10 nm radius Pt NP on Bi, the mass transfer rate of proton is  $m = D_H^+/r_{NP} = (9.3 \times 10^{-5} \text{ cm}^2/\text{s})/(1 \times 10^{-5} \text{ cm}^2/\text{s})$  $10^{-6}$  cm) = 93 cm/s, which is much larger than the fitted  $k^0 \approx 0.1$ cm/s. Consequently, the voltammogram can be irreversible, and the  $k^0$  value for the curve fitting is unique. For other particles on Bi, no special concern in the fitting accuracy is needed due to smaller size (i.e., faster diffusion) and slower kinetics.

For Bi and Pb substrates, when the particle radius increased the HER kinetics increased until a limiting plateau was reached; this was attained when the NP size was about 4 nm (Figure 5C.D). The enhanced activity with increasing particle size might be attributed to changes in the H<sup>•</sup> adsorption energy. <sup>21,27,28</sup> The limiting  $k^0$  for the Bi substrate is ca.  $10^{-1}$  cm/s that is close to the previously reported  $\sim$ 0.3 cm/s at bulk Pt,  $^{20}$  while for the Pb substrate it is sluggish at ca.  $10^{-4}$  cm/s.

Figure 6 shows the extracted  $k^0$  as a function of the radius of a single Pt deposit on Bi and Pb substrates. We infer that a

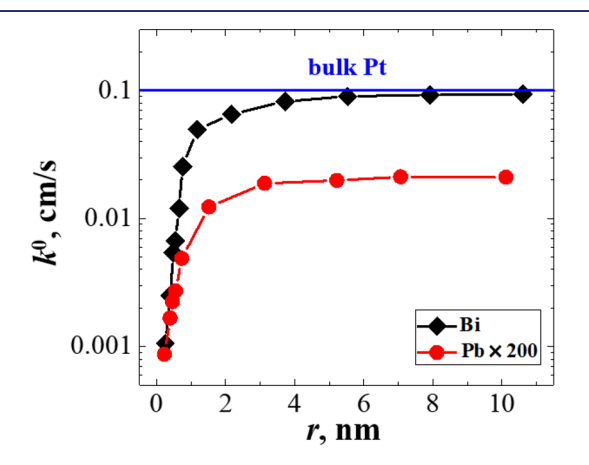


**Figure 6.** Extracted  $k^0$  as a function of the radius of a single Pt deposit on Bi and Pb substrates and the value at the dashed line is taken for the HER kinetics at bulk Pt. For comparison, the kinetic constants on Pb are magnified by 200 times.

comparable size of single Pt electrodeposits on Bi and Pb showed a largely different activity caused by a strong interaction of the Pt with the substrate. $^{29-32}$  There have been many studies of catalyst/support interactions, for example SMSI (strong metal-support interactions). These interactions involve charge-transfer (ligand) effects, structural (e.g. stress) effects, and other factors, such as hydrogen spillover. An understanding of the effects seen here must await further studies.

Moreover, we find that for the same substrate, the electrocatalytic activity of a single Pt atom is only 1% of that of a large Pt NP. Sun et al. prepared arrays of single platinum atoms and clusters supported on nitrogen-doped graphene nanosheets by ALD, and then characterized the HER on the catalyst film (i.e., materials confined in a Nafion matrix) by rotating disk electrode voltammetry. By estimating the current density at a given potential, they claimed that the catalytic activity of isolated single Pt atoms was much higher than that of commercial bulk Pt NP catalysts. However, their calculated current density was normalized by the geometric area of a rotating disk electrode rather than the electrochemically active surface area. Our approach with single isolated Pt atoms probably gives a better estimate of current density, an important parameter in any kinetic treatment.

#### CONCLUSIONS

In summary, we prepared a wide size range of single Pt deposits on Bi and Pb UMEs by a finely controlled electrodeposition, where the formed single atoms, atomic clusters, and NPs were extensively tested for a catalytic HER. The electrochemical evaluations obtained on these individual deposits produced steady-state sigmoidal shapes of voltammograms. By fitting the theoretical equations to these curves, the HER kinetics are extracted to examine the correlations of the particle-size and the supporting substrate to the electrocatalytic activity. To the best of our knowledge, the present study is a first demonstration using a single isolated particle approach to clarify the key catalytic factors, rather than the conventional measurement of particle ensembles.

#### ASSOCIATED CONTENT

# Supporting Information

The Supporting Information is available free of charge on the ACS Publications website at DOI: 10.1021/jacs.8b13366.

Experimental details such as chemicals and materials, preparation of ultradiluted H2PtCl6 solution, fabrication of Bi and Pb UMEs, and electrochemical plating, detection, instrumentation, and simulation (PDF)

#### AUTHOR INFORMATION

### **Corresponding Author**

\*ajbard@cm.utexas.edu

ORCID 0

Allen J. Bard: 0000-0002-8517-0230

The authors declare no competing financial interest.

# ACKNOWLEDGMENTS

We acknowledge support of this research from the National Science Foundation (CHE-1405248, A.J.B.) and the Robert A. Welch Foundation (F-0021).

# REFERENCES

- (1) Zhou, M.; Dick, J. E.; Bard, A. J. Electrodeposition of Isolated Platinum Atoms and Clusters on Bismuth: Characterization and Electrocatalysis. J. Am. Chem. Soc. 2017, 139, 17677.
- (2) Kim, J.; Dick, J. E.; Bard, A. J. Advanced electrochemistry of individual metal clusters electrodeposited atom by atom to nanometer by nanometer. Acc. Chem. Res. 2016, 49, 2587.
- (3) Qiao, B.; Wang, A.; Yang, X.; Allard, L. F.; Jiang, Z.; Cui, Y.; Liu, J.; Li, J.; Zhang, T. Single-atom catalysis of CO oxidation using Pt<sub>1</sub>/FeO<sub>x</sub>. Nat. Chem. 2011, 3, 634.
- (4) Deng, J.; Li, H.; Xiao, J.; Tu, Y.; Deng, D.; Yang, H.; Tian, H.; Li, J.; Ren, P.; Bao, X. Triggering the electrocatalytic hydrogen evolution activity of the inert two-dimensional MoS<sub>2</sub> surface via single-atom metal doping. Energy Environ. Sci. 2015, 8, 1594.
- (5) Cheng, N.; Stambula, S.; Wang, D.; Banis, M. N.; Liu, J.; Riese, A.; Xiao, B.; Li, R.; Sham, T.-K.; Liu, L.-M.; Botton, G. A.; Sun, X. Platinum single-atom and cluster catalysis of the hydrogen evolution reaction. Nat. Commun. 2016, 7, 13638.
- (6) Zhu, C.; Fu, S.; Shi, Q.; Du, D.; Lin, Y. Single-Atom Electrocatalysts. Angew. Chem., Int. Ed. 2017, 56, 13944.
- (7) Proch, S.; Wirth, M.; White, H. S.; Anderson, S. L. Strong effects of cluster size and air exposure on oxygen reduction and carbon oxidation electrocatalysis by size-selected Ptn ( $n \le 11$ ) on glassy carbon electrodes. J. Am. Chem. Soc. 2013, 135, 3073.
- (8) Arán-Ais, R. M.; Yu, Y.; Hovden, R.; Solla-Gullón, J.; Herrero, E.; Feliu, J. M.; Abruña, H. D. Identical Location Transmission Electron

- Microscopy Imaging of Site-Selective Pt Nanocatalysts: Electrochemical Activation and Surface Disordering. *J. Am. Chem. Soc.* **2015**, 137, 14992.
- (9) Nesselberger, M.; Roefzaad, M.; Hamou, R. F.; Biedermann, P. U.; Schweinberger, F. F.; Kunz, S.; Schloegl, K.; Wiberg, G. K.; Ashton, S.; Heiz, U. The effect of particle proximity on the oxygen reduction rate of size-selected platinum clusters. *Nat. Mater.* **2013**, *12*, 919.
- (10) Gara, M.; Ward, K. R.; Compton, R. G. Nanomaterial modified electrodes: evaluating oxygen reduction catalysts. *Nanoscale* **2013**, *S*, 7304.
- (11) Huang, J.; Zhang, J.; Eikerling, M. H. Particle proximity effect in nanoparticle electrocatalysis: surface charging and electrostatic interactions. *J. Phys. Chem. C* **2017**, *121*, 4806.
- (12) Leonard, K. C.; Bard, A. J. Pattern recognition correlating materials properties of the elements to their kinetics for the hydrogen evolution reaction. *J. Am. Chem. Soc.* **2013**, *135*, 15885.
- (13) Xiao, X.; Bard, A. J. Observing Single Nanoparticle Collisions at an Ultramicroelectrode by Electrocatalytic Amplification. *J. Am. Chem. Soc.* **2007**, *129*, 9610.
- (14) Chen, S.; Kucernak, A. Electrodeposition of Platinum on Nanometer-Sized Carbon Electrodes. *J. Phys. Chem. B* **2003**, *107*, 8392. (15) Oldham, K. B.; Zoski, C. G. Comparison of voltammetric steady states at hemispherical and disc microelectrodes. *J. Electroanal. Chem. Interfacial Electrochem.* **1988**, *256*, 11.
- (16) Ma, W.; Hu, K.; Chen, Q.; Zhou, M.; Mirkin, M. V.; Bard, A. J. Electrochemical size measurement and characterization of electrodeposited platinum nanoparticles at nanometer resolution with scanning electrochemical microscopy. *Nano Lett.* **2017**, *17*, 4354.
- (17) Qian, H.; Zhu, M.; Wu, Z.; Jin, R. Quantum Sized Gold Nanoclusters with Atomic Precision. *Acc. Chem. Res.* **2012**, 45, 1470.
- (18) Liu, Y.; He, R.; Zhang, Q.; Chen, S. Theory of Electrochemistry for Nanometer-Sized Disk Electrodes. *J. Phys. Chem. C* **2010**, *114*, 10812.
- (19) Fernández, J. L.; Zoski, C. G. Voltammetric and Scanning Electrochemical Microscopy Investigations of the Hydrogen Evolution Reaction in Acid at Nanostructured Ensembles of Ultramicroelectrode Dimensions: Theory and Experiment. J. Phys. Chem. C 2018, 122, 71.
- (20) Zoski, C. G. Scanning Electrochemical Microscopy: Investigation of Hydrogen Oxidation at Polycrystalline Noble Metal Electrodes. *J. Phys. Chem. B* **2003**, *107*, 6401.
- (21) Zheng, Y.; Jiao, Y.; Jaroniec, M.; Qiao, S. Z. Advancing the Electrochemistry of the Hydrogen-Evolution Reaction through Combining Experiment and Theory. *Angew. Chem., Int. Ed.* **2015**, *54*, 52.
- (22) Heerman, L.; Tarallo, A. Electrochemical nucleation on microelectrodes. Theory and experiment for diffusion-controlled growth. *J. Electroanal. Chem.* **1998**, 451, 101.
- (23) Velmurugan, J.; Noël, J.-M.; Nogala, W.; Mirkin, M. V. Nucleation and growth of metal on nanoelectrodes. *Chem. Sci.* **2012**, 3, 3307.
- (24) Kim, J.; Bard, A. J. Electrodeposition of Single Nanometer-Size Pt Nanoparticles at a Tunneling Ultramicroelectrode and Determination of Fast Heterogeneous Kinetics for Ru (NH<sub>3</sub>)<sub>6</sub><sup>3+</sup> Reduction. *J. Am. Chem. Soc.* **2016**, *138*, 975.
- (25) Hussein, H. E. M.; Maurer, R. J.; Amari, H.; Peters, J. J. P.; Meng, L.; Beanland, R.; Newton, M. E.; Macpherson, J. V. Tracking Metal Electrodeposition Dynamics from Nucleation and Growth of a Single Atom to a Crystalline Nanoparticle. *ACS Nano* **2018**, *12*, 7388.
- (26) Ustarroz, J.; Hammons, J. A.; Altantzis, T.; Hubin, A.; Bals, S.; Terryn, H. A Generalized Electrochemical Aggregative Growth Mechanism. *J. Am. Chem. Soc.* **2013**, *135*, 11550.
- (27) Zheng, J.; Zhou, S.; Gu, S.; Xu, B.; Yan, Y. Size-dependent hydrogen oxidation and evolution activities on supported palladium nanoparticles in acid and base. *J. Electrochem. Soc.* **2016**, *163*, F499.
- (28) Ohyama, J.; Sato, T.; Yamamoto, Y.; Arai, S.; Satsuma, A. Size specifically high activity of Ru nanoparticles for hydrogen oxidation reaction in alkaline electrolyte. *J. Am. Chem. Soc.* **2013**, *135*, 8016.
- (29) Du, M.; Cui, L.; Cao, Y.; Bard, A. J. Mechanoelectrochemical catalysis of the effect of elastic strain on a platinum nanofilm for the

- ORR exerted by a shape memory alloy substrate. J. Am. Chem. Soc. 2015, 137, 7397.
- (30) Li, H.; Du, M.; Mleczko, M. J.; Koh, A. L.; Nishi, Y.; Pop, E.; Bard, A. J.; Zheng, X. Kinetic study of hydrogen evolution reaction over strained MoS<sub>2</sub> with sulfur vacancies using scanning electrochemical microscopy. *J. Am. Chem. Soc.* **2016**, 138, 5123.
- (31) Liu, Y.; Mustain, W. E. High Stability, High Activity Pt/ITO Oxygen Reduction Electrocatalysts. *J. Am. Chem. Soc.* **2013**, *135*, 530.
- (32) Lu, Y.; Jiang, Y.; Gao, X.; Wang, X.; Chen, W. Strongly Coupled Pd Nanotetrahedron/Tungsten Oxide Nanosheet Hybrids with Enhanced Catalytic Activity and Stability as Oxygen Reduction Electrocatalysts. J. Am. Chem. Soc. 2014, 136, 11687.